Secondary craters of Tycho: Size-frequency distributions and estimated fragment size–velocity relationships

Naru Hirata[1] and Akiko M. Nakamura[1]

[1]   We examined the size-frequency distribution and the spatial distribution of secondary craters around the lunar crater Tycho. Secondary crater diameters were found to range from 0.55 to 4.0 km, and their distance from Tycho to range from 130 to 370 km. The diameter and ejection velocity of the secondary-forming fragments were also estimated from the crater size and the distance from the primary using the scaling relationships for cratering. The power law index of the size-frequency distribution of the Tycho secondary craters ranges from 3.3 to 4.0, the same as the steep slope of the typical size-frequency distribution for lunar craters of less than 4 km diameter. The decay index of secondary crater densities with distance from the primary craters is not constant and is small at large distances (less than 2.5 for r > 2.5R). The total number of secondaries forming ejecta fragments is more than twice larger than for other lunar primaries previously studied. These results imply that there are many small secondary craters in fields far from the primary crater. A dominant contribution of secondaries to the size-frequency distribution of all lunar craters is thus strongly suggested. The index range of 2.6 to 3.0 for estimated fragment size distributions is not only close to other natural and experimental craters, but also to those of blocks on asteroids. The relative fragment size distributions are independent of the ejection velocity. This result is the first observational confirmation of the theoretical assumption, and agrees with a recent result from laboratory experiments.

1.   Introduction

[2]   When an impact occurs on a planetary surface, many fragments ejected from the primary crater fall back to the surface and form secondary craters. Understanding the nature of secondary craters is important for many aspects of planetary science. One of the most controversial issues is the effect of secondary craters on crater chronology [e.g., *Shoemaker*, 1965; *Neukum and Ivanov*, 1994; *McEwen*, 2003; *Namiki and Honda*, 2003; *Hartmann*, 2005]. The crater size–frequency distributions on the Moon, Mars, and other small bodies develop a steep branch at a particular crater diameter (less than 4 km on the Moon). The question of whether these small craters are dominated by primary impacts or by secondary impacts is critical to obtaining age constraints using crater counting techniques, especially on young or small terrains containing only a few craters.

[3]   The ejection velocities and diameters of the ejecta fragments that produced the secondaries can be estimated from their radial range from the primary crater and the size of the secondaries [*Vickery*, 1986, 1987; *Hirase et al.*, 2004] by applying a scaling relationship [*Holsapple and Schmidt*, 1982]. The size-velocity relation of impact ejecta is a funda-

mental part of studies investigating the collisional evolution of asteroids and the ejection of meteorites from large bodies. In addition, a comprehensive understanding of the size-velocity relation of impact ejecta is also essential to the subject of secondary cratering.

[4]   We present the results of analyses of secondary craters around the lunar crater Tycho in order to derive the size-frequency distribution, the spatial distribution of secondary craters, and the size-velocity relation of ejecta fragments. Previous analyses of secondary craters were insufficient by comparison: some presented only a single size-frequency distribution of all secondaries around a primary; others focused on the maximum size of secondaries within a certain range from the primary; some included all craters without distinction between small primaries and secondaries. In this analysis, secondaries were separated from small primaries, and measurements of the size and range from the primary source were performed for each secondary crater. Tycho (D = 85 km) is one of the freshest large craters on the Moon. Apart from some studies on its distant ray system and associated secondary craters [*Shoemaker*, 1965; *Arvidson et al.*, 1976], there has been no previous report on the secondary crater distribution around Tycho.

2.   Method

[5]   We used the images in the USGS Clementine UVVIS 750-nm Lunar Digital Image Model data set [*Isbell et al.*,

---

[1]Graduate School of Science and Technology, Kobe University, Kobe, Japan.
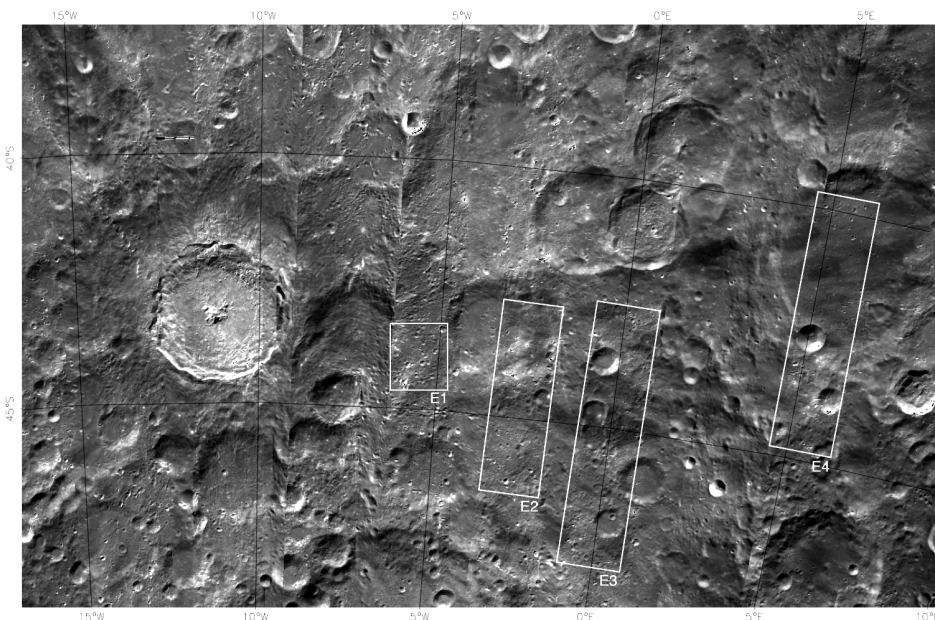
Figure 1. A mosaic image of Tycho crater and its eastern secondary crater field. The locations of the four analyzed regions, E1, E2, E3, and E4, are indicated.

1999] for this analysis. Image data were reassembled into a large mosaic over an azimuthal equal area projection centered on Tycho. Although the resolution of the mosaicked image was 100 m/pixel, the effective resolution within the image varied from 100 up to 800 m/pixel. This variation in spatial resolution was mainly due to differences in the observation altitude of the Clementine spacecraft during the mapping operation. Four regions to the east of Tycho were selected for detailed analysis from areas with the best effective resolution. Their locations are shown in Figure 1, and a summary is given in Table 1.

[6] The identification of secondary craters is based on their morphological characteristics [*Wilhelms et al.*, 1978; *Melosh*, 1989]. Some examples of typical secondary craters of Tycho are shown in Figure 2. Compared with primary craters, secondaries are less circular. Some also have characteristic chevron-shaped herringbone rim patterns. Secondaries are shallower than primary craters, and their inner profiles are irregular. The slopes on the side closest to the primary crater are steeper, whereas the walls on the opposite side are shallower. Consequently, the rims on the opposite side are often faint and hard to recognize. It is also common to find hummocks on the floors of secondaries. As many secondaries tend to form chains or clusters, such features also provide strong clues to their identification [*Melosh*,

1989]. However, it is necessary to confirm whether the directions of chains and elongated distributions of clusters point to the primary crater, Tycho, to distinguish between the Tycho secondaries and secondaries from other craters or primary crater chains. In contrast to typical secondary morphologies, small, very regular bowl-shaped craters with sharp rims were assumed to be small primaries. The characteristic features of secondaries described here are caused mainly by the relatively low impact velocity of the fragments [*Melosh*, 1989] and the interference between adjacent secondaries that are simultaneously produced [*Oberbeck and Morrison*, 1973]. The impact velocity becomes higher with increased distance from the primary crater, and the density of the fragments also decreases. Hence a distinction between secondaries and primaries is difficult at large distances from the primary crater, especially on small craters. We also supplementary used an optical maturity map derived from Clementine UVVIS multiband images [*Grier et al.*, 2001; *Hirata et al.*, 2004]. Although a difference of optical maturity of a secondary crater relative to other craters is not so apparent, it is useful to confirm a secondary crater is not so old and mature. Many rays are observed in the optical maturity map as streaks of immature materials associated to clusters or chains of secondaries [*Hirata et al.*, 2004].

Table 1. Summary of Analyzed Regions and Results

Region	Range From Tycho,[a] km	Size of Region, km	Area, km²	Number of Secondaries	Best-Fit Power Law Relation	Estimated U, m/s	Power Law Index of Fragment Size
E1	130 (3.1R)[b]	33.6 × 40.0	1344	92 (35)[c]	$N(>D) = 1.32 \pm 0.11 \times 10^{-1} D^{-3.44 \pm 0.11}$	420–470	−2.69 ± 0.09
E2	190 (4.5R)	37.9 × 116.2	4404	145 (52)	$N(>D) = 1.26 \pm 0.07 \times 10^{-2} D^{-3.82 \pm 0.15}$	510–575	−2.98 ± 0.12
E3	250 (5.9R)	41.0 × 162.7	6650	134 (48)	$N(>D) = 6.65 \pm 0.18 \times 10^{-3} D^{-3.32 \pm 0.07}$	590–640	−2.59 ± 0.05
E4	370 (8.7R)	39.1 × 156.3	6111	98 (43)	$N(>D) = 6.81 \pm 0.20 \times 10^{-3} D^{-3.34 \pm 0.09}$	720–750	−2.61 ± 0.07

[a]Distance at the center of the region.
[b]Normalized by Tycho diameter 85 km.
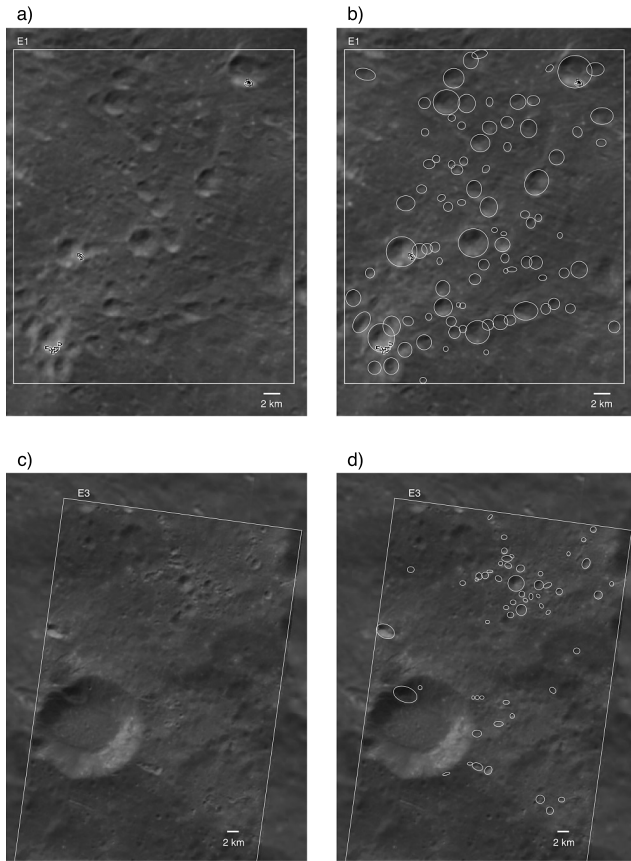[c]Number of secondaries used for curve fitting.

Figure 2. Some examples of secondary craters in the analyzed regions. (a) A view of secondary craters in the region E1 and (b) the same view with outlines of secondaries. (c) A view of the northern half of the region E3 and (d) the same view with outlines of secondaries. Geometric patterns of black-and-white pixels in the images are artifacts due to image resampling.

[7] We excluded doubtful craters from our counting of secondary craters of Tycho, so that our results provide lower limits. To evaluate the effects of misclassification between primaries and secondaries, a counting of all craters in the target regions irrespective of classification as primary or secondary was also conducted (Figure 3). The best-fit power law is also shown in the figure. The highlands to the east of Tycho were interpreted as having a pre-Nectarian age [*Wilhelms*, 1987]. The result is in agreement with a previous crater counting study of other pre-Nectarian terrains [*Neukum*, 1977]. A detailed evaluation is presented in the next section.

[8] Diameters of secondaries are defined as the minor axis diameter of the ellipse fitted to the crater rim. Distances from the center of Tycho were also measured. Ejection velocities and ejecta size were derived by a method similar to that of *Vickery* [1986, 1987] and *Hirase et al.* [2004]. The ejection velocity is given by the range-velocity equation for a spherical surface,

$$U = \frac{\sqrt{R_{moon} g_{moon}} \tan(R/2R_{moon})}{\sqrt{\tan(R/2R_{moon}) \cos^2 \theta + \sin \theta \cos \theta}}, \quad (1)$$

where R_{moon} and g_{moon} are the radius and surface gravity, and R is the distance from the center of the primary.

[9] The ejection angle and the incidence angle were both assumed to be 45 degrees. The ejecta diameter was estimated from the ejection velocity and the secondary crater diameter by applying a scaling relationship [*Holsapple and Schmidt*, 1982]. We used the gravity scaling relationship for a nonporous regolith target [*Vickery*, 1986, equation (1)],

$$d = 0.753 D^{1.28} (\sin \theta)^{-1/3} (g_{moon}/U^2)^{0.277}. \quad (2)$$

The transition diameter of ejecta fragment from the strength regime to the gravity regime on the Moon is about 60 m according to *Vickery* [1986], so that all secondaries are in the gravity regime.

3. Size-Frequency Distributions of Secondary Craters

[10] We counted 92, 145, 134, and 98 secondary craters in the regions E1, E2, E3, and E4, respectively. The range of crater diameters is from 550 m to 4.0 km. The cumulative size-frequency distributions of secondary craters are shown in Figure 4. All distributions show shallow slopes at small sizes. The inflection points of the distributions are at 1.7 km diameter in region E1, and 1 km diameter in regions E2, E3, and E4. In Figure 4, we also show best fits for secondaries with diameters greater than the inflection points with power laws,

$$N_{crater}(\geq D) = cD^{-b}, \quad (3)$$

where $N_{crater}(\geq D)$ is a cumulative number of secondary craters per km^2 with diameters greater than or equal to D, b is a power law index, and c is a constant factor. The indices b of the fitted lines are 3.44 ± 0.11, 3.82 ± 0.15, 3.32 ± 0.07, and 3.34 ± 0.09 in regions E1, E2, E3, and E4, respectively.
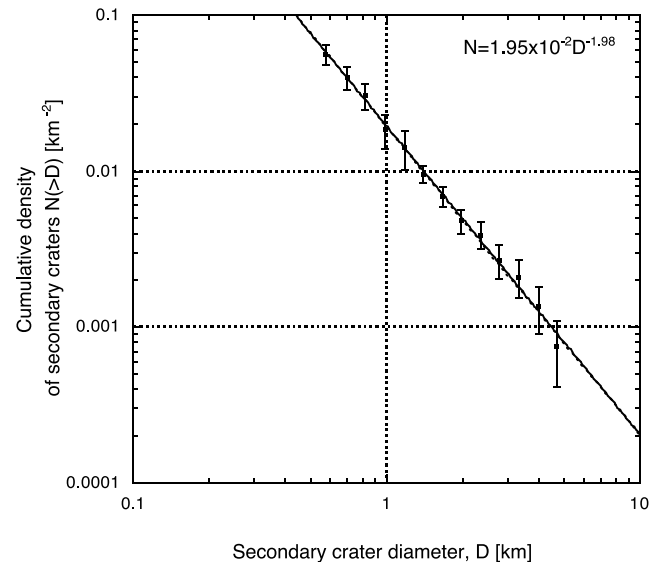

Figure 3. Size-frequency distribution of both primary and secondary craters in the region E2. The solid line is the best power law fit.
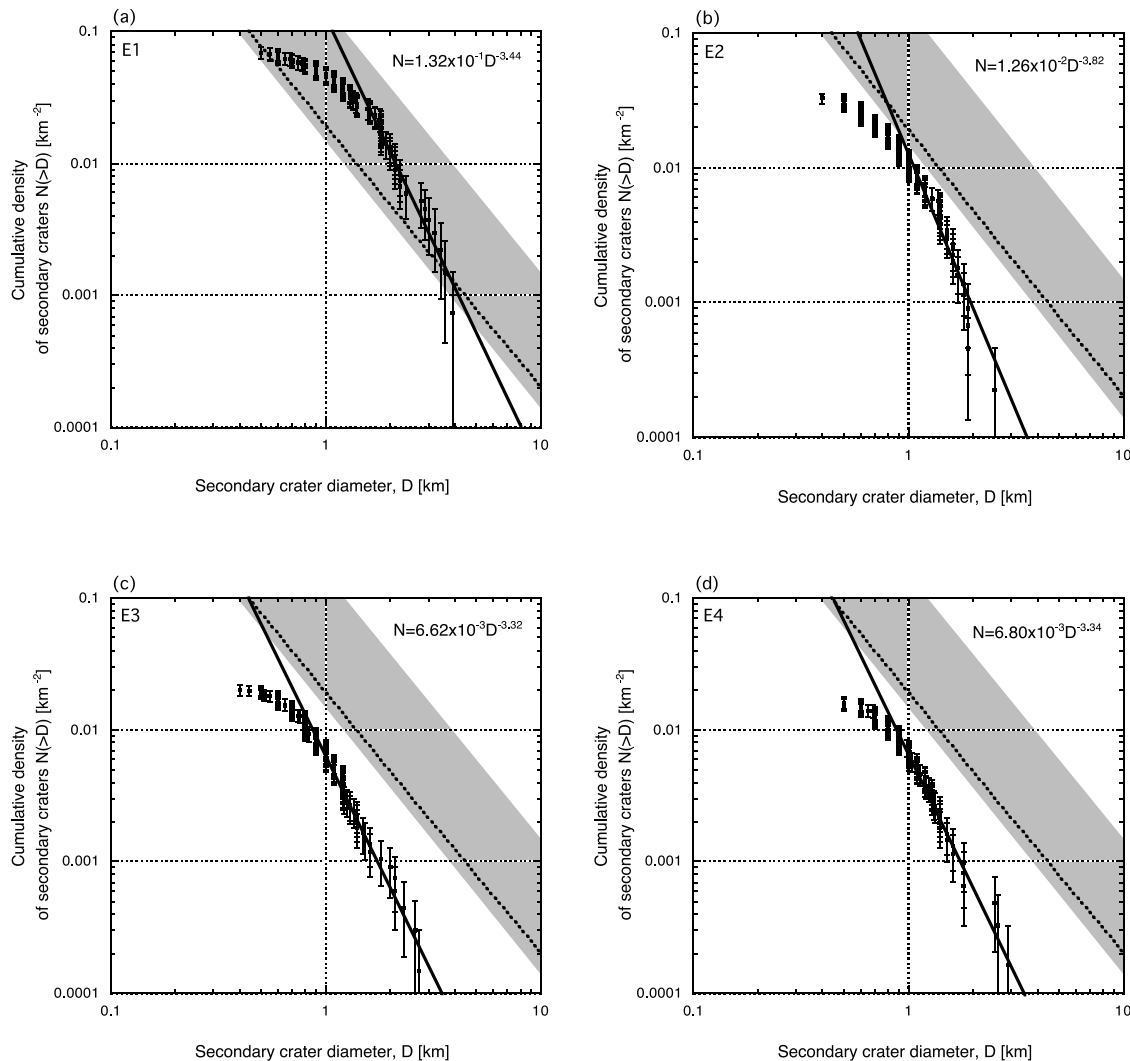
Figure 4. Size-frequency distributions of secondary craters around Tycho in three analyzed regions. The solid lines are the best power law fits for secondaries larger than 1.7 km, 1.0 km, and 1.0 km in the regions E1, E2, and E3, respectively. The dashed line is the size-frequency distribution of both primary and secondary craters in the region E2. The shaded band indicates crater equilibrium for which the factor *c* is between 0.15 and 0.015 [*Melosh*, 1989; *Namiki and Honda*, 2003].

Results of the analysis of the size-frequency distributions are summarized in Table 1.

[11] In Figure 4, the fitting curve for both primary and secondary craters at the region E2 is also shown as a baseline to evaluate effects of misclassification between primaries and secondaries. In the region E1, the density of secondary craters is very high, and most data points are above the baseline. The morphological characteristics of secondaries are also very distinctive in this region, so the effect of contamination from primaries is minor. However, all of the data points in the other three regions are below the baseline. As the secondary counting criteria in this study are very strict, the cumulative densities of secondary craters shown here are lower limits. The majority of misclassifications of secondaries as primaries are expected to occur with smaller craters, while larger ones are easily classified as either primaries or secondaries. It therefore seems likely that the fitting results give lower limits of the power law indices. If we compare the baseline and secondary counting results

at a diameter of 1 km, the minimum diameter of curve fitting, the possible maximum of the secondary densities is about three times higher than the actual counts. The possible maximum of the power law index is also around 4.

[12] *Shoemaker* [1965] studied the size-frequency distributions of secondary craters for terrestrial explosion craters and lunar craters. The power law index of secondaries of the Sedan nuclear explosion crater (D = 400 m) is about 4.0, and that of the lunar crater Langrenus (D = 131 km) is also about 4.0, based on ground-based telescopic observations. The secondary crater field of Tycho in Mare Cognitum has a value slightly less than 4.0 from Ranger 7 spacecraft images. The secondary crater field in Mare Cognitum is located about 1000 km north of Tycho. *Wilhelms et al.* [1978] reported a power law index of 3.6 for basin (Imbrium basin and Orientale basin) secondaries larger than 7 km in diameter. The values of the power law indices in this study are in good agreement with the values of secondaries of large basins. Although the values reported
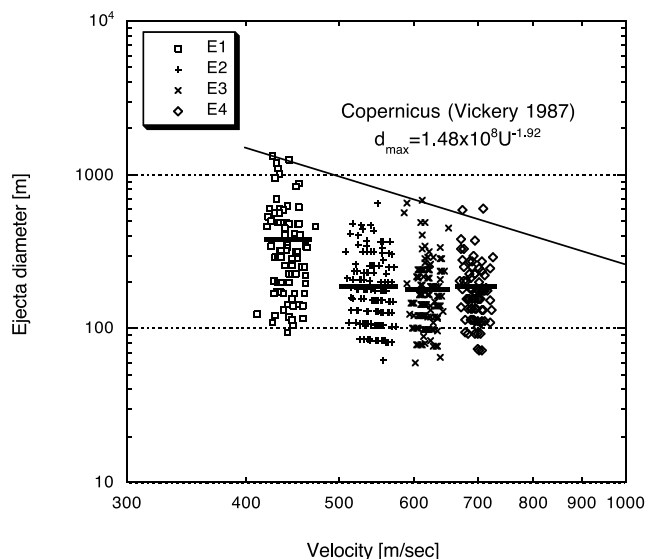
Figure 5. Estimated size-velocity relation of ejecta fragments. Short horizontal bars indicate mean fragment diameters. A curve of maximum size of ejecta fragments versus velocity derived from secondaries of Copernicus crater [*Vickery*, 1987] is also shown.

by *Shoemaker* [1965] are slightly higher than our best fit, a power law function of index 4.0 falls on our distribution plot within the error bars. We can conclude that the power law index of secondaries is in the range between 3.3 and 4.0, certainly higher than the index of 1.8 for primaries larger than 4 km in diameter [*Basaltic Volcanism Study Project*, 1981; *Namiki and Honda*, 2003]. Results of our study and previous reports show that the index depends neither on the distance from the primary crater nor the size of the primary crater.

[13] The shallow distribution slopes of smaller craters are not caused by observational incompleteness, but by obliteration of other secondaries. The diameters at which the slopes become shallower are much larger than the effective image resolution of 100 m/pixel within the studied regions. The cumulative density of secondaries in the region E1 is within the range of the equilibrium density suggested by *Melosh* [1989] (Figure 4a). When many secondaries form simultaneously within a small area, surges of combined primary and secondary ejecta obliterate some of the small secondaries. The region E1 is near a continuous ejecta blanket where the ballistic sedimentation process is dominant and all secondaries are obliterated [*Oberbeck*, 1975] and so obliteration should be important here. In the regions E2, E3, and E4, the average secondary densities of the entire region are below the equilibrium; however, even in these regions, the local density of secondaries that form clusters is high, and the process of obliteration is still shown to be effective. Such obliteration was even observed in a more distant secondary crater field of Tycho [*Arvidson et al.*, 1976], and in secondaries of large impact basins [*Wilhelms et al.*, 1978].

[14] The power law factor c varies with distance from the primary crater. The measured value of c, 1.32×10^{-1}, is very high in the region nearest to the primary crater, E1,

whereas it has decreased by an order of magnitude to 1.26×10^{-2} in region E2. The factor c is still decreasing from region E2 to E3, but more gently than for a nearby region by a factor of about 2. It then becomes almost constant in the range from 6.65×10^{-3} to 6.81×10^{-3} for regions E3 and E4. Such a tendency is not as apparent on other lunar craters Alencar, Copernicus, and Aristarchus [*Schultz and Singer*, 1980]. One implication of this result will be discussed in the next section with an estimation of the mass of ejecta fragments.

4. Size-Velocity Relationships and Mass of Ejecta Fragments

[15] In this section, the size and velocity distributions of the ejecta fragments that produced the secondary craters will be discussed. Size-velocity relationships of ejecta fragments estimated using equations (1) and (2) are shown in Figure 5. The ejection velocity ranges are 420–470 m/s at E1, 510–575 m/s at E2, 590–640 m/s at E3, and 720–750 m/s at E4. The curve shows the relationship between the maximum fragment diameter d_{max} and the ejection velocity U obtained by *Vickery* [1987] for the Copernicus crater (D = 93 km) with a diameter close to that of Tycho. The new $d_{max}-U$ relationships for Tycho may be fitted by a power law, similar to that of Copernicus. However, it should be noticed that mean fragment sizes, which are shown as short, thick horizontal bars in Figure 5, are almost the same for regions E2, E3, and E4. This trend reflects the results for secondary crater densities.

[16] The fragment size data are also shown in cumulative size–frequency distribution plots (Figure 6). Since the scaling laws given by equation (2) relate projectile diameter and crater diameter, the power index of the fragment size–
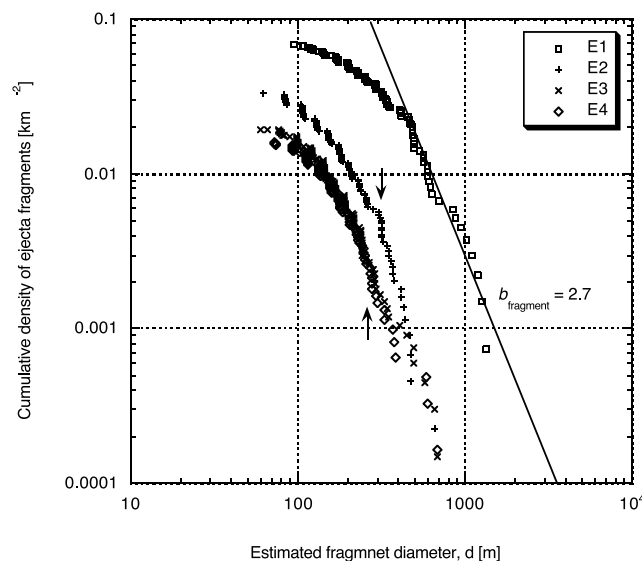

Figure 6. Estimated size-frequency distributions of secondary fragments of Tycho in the four analyzed regions. The cumulative numbers of fragments are normalized by the range of ejection velocity and that of radial extent angle from the center of the primary crater. The solid line is a power law of index 2.6. The arrows show inflection points in the size-frequency distributions at 300 m diameter.

frequency distribution $b_{fragment}$ can be obtained from that of secondary crater size b by

$$b_{fragment} = \frac{b}{1.28}, \qquad (4)$$

where a divisor 1.28 comes from the exponent in equation (2). Derived power law indices $b_{fragment}$ in regions E1, E2, E3, and E4 are 2.69 ± 0.09, 2.98 ± 0.12, 2.59 ± 0.05, and 2.61 ± 0.07, respectively. We note that these indices are for fragments with diameters larger than the inflection points of the crater size distributions. All indices range from 2.6 to 3.0, and are independent of ejection velocity.

[17] *O'Keefe and Ahrens* [1985] developed a theoretical model of the size–velocity distribution of crater ejecta fragments. By comparing the model calculations with observed fragment size distributions and the $d_{max} - U$ relations, they concluded that the size distribution of ejecta at a given velocity is very broad. In other words, the relative size distribution of crater ejecta is not dependent on the ejection velocity. Our result is the first observational confirmation of this suggestion. A laboratory experiment by *Michikami et al.* [2005] also showed the same result.

[18] If the relative fragment size distribution is completely independent of ejection velocity, the power index of the ejecta fragments is the same as the index observed at a given velocity, as obtained in this study. The power index of all ejecta fragments is found to be in the range of 2.45 and 2.6 for laboratory-scale craters and explosion craters [e.g., *Gault et al.*, 1963; *Fujiwara et al.*, 1977; *O'Keefe and Ahrens*, 1985]. The results for Tycho are in good agreement with the experimental results.

[19] The power law index of the size distribution of the fragments is close to the index 2.5 for the distribution of ejecta blocks on the surface of the asteroid Eros [*Thomas et al.*, 2001; *Cheng*, 2004]. *Thomas et al.* [2001] proposed that most ejecta blocks on Eros originally come from the Shoemaker crater (D = 7.6 km). This result suggests that the 2.5–3.0 index power law governs impact cratering events over a wide range of primary crater sizes.

[20] Even though the fragment size distributions can be broadly fit by power laws, it is notable that there are several inflection points in the size distribution of ejecta fragments. The inflection point in the cumulative distribution curve means that there are many fragments with the same diameter. The most evident inflection points are for fragments around 300 m in diameter for E2, E3, and E4 (the arrows in Figure 6). The distribution in region E1 also has a minor inflection point at the same diameter. This suggests that the fragmentation process produces a characteristic size of fragments. The secondary-producing fragments are ejected by a spall process [*Melosh*, 1984, 1989]. *Melosh* [1984] assumed a mean fragment diameter as a function of ejection velocity, tensile strength of the target, and projectile diameter. If we adopt a projectile diameter of 6.6 km for Tycho [*Cintala and Grieve*, 1998] and the dynamic tensile strength of the target material (0.1 GPa [*Melosh*, 1984]), the estimated fragment diameter ranges from 1300 to 700 m for ejection velocities of 450 and 750 m/s, respectively. These values are larger than those in Figure 6, but quite close to the maximum fragment diameter for each region. It is possible that fragmentation of larger blocks occurred during

spallation and subsequent ballistic flight, or that the tensile strength was weaker than that assumed.

[21] The data obtained in this study allow us to discuss not only the relative size–frequency distributions of ejecta fragments, but also their absolute volume and mass. *Haskin et al.* [2003] developed a model for estimation of thickness of ejecta and ejecta deposits by using scaling relationships. We modified their model to obtain the thickness of ejecta material from the size-frequency distribution of secondary craters. If a mass-frequency distribution of ejecta fragments follows a power law,

$$N_{mass}(\geq m) = c_{mass} \cdot m^{-b_{mass}}, \qquad (5)$$

then the total mass of ejecta M_T is given by

$$M_T = c_{mass} \frac{b_{mass}}{b_{mass} - 1} \left(m_{max}^{1-b_{mass}} - m_{min}^{1-b_{mass}} \right), \qquad (6)$$

where m_{max} and m_{min} are upper and lower limits of integration. From equations (2)–(5), the constants of the power function of ejecta mass and are also expressed as

$$b_{mass} = \frac{b_{fragment}}{3} = \frac{b}{3 \times 1.28} \qquad (7)$$

$$c_{mass} = c \cdot \left[\frac{1}{6} \cdot \pi \cdot \rho \cdot \left\{ 0.753 D^{1.28} (\sin \theta)^{-1/3} (g_{moon}/U^2)^{0.277} \right\}^3 \right]^{b_{mass}}. \qquad (8)$$

The maximum mass of fragments is obtained from the diameter of the largest secondary crater at each region. We used a density ρ of 3000 kg/m³, and a m_{min} of 0.001 g, following *Haskin et al.* [2003]. Even though there is no direct evidence to confirm that a power law distribution of ejecta fragments is satisfied at that small size, some contribution of small fragments in a secondary crater field is suggested by the distribution of bright immature materials and ray systems around Tycho [*Grier et al.*, 2001; *Hirata et al.*, 2004]. If integration is stopped at a mass of 1×10^{-9} kg, corresponding to a fragment with diameter 100 m, the normalized thickness of ejecta fragment t/R may decrease by about 60% in the regions E1, E3, and E4. In the region E2, the decrease is larger than other regions, only 18% of the nominal value, because of its larger power index.

[22] Predicted ejecta thickness normalized with the primary crater radius is presented in Figure 7. Error bars on the plot are from the uncertainty in the power law index of the crater size–frequency distribution b. Figure 7 also illustrates the model ejecta thickness suggested by *McGetchin et al.* [1973]. As already discussed in the previous section, the fragments that form secondary craters are considered to be spall fragments. It is generally thought that most ejecta material is fine-grained ejecta excavated and ejected from a transient cavity [*Oberbeck*, 1975; *Hörz et al.*, 1983; *Melosh*, 1989], and the contribution of secondary-crater-forming fragments to the total volume of crater ejecta is considered to be minor. An overall trend seems to follow with a power law of index 3.0 in the regions E1 and E2, although the predicted ejecta thickness is slightly lower than in the model
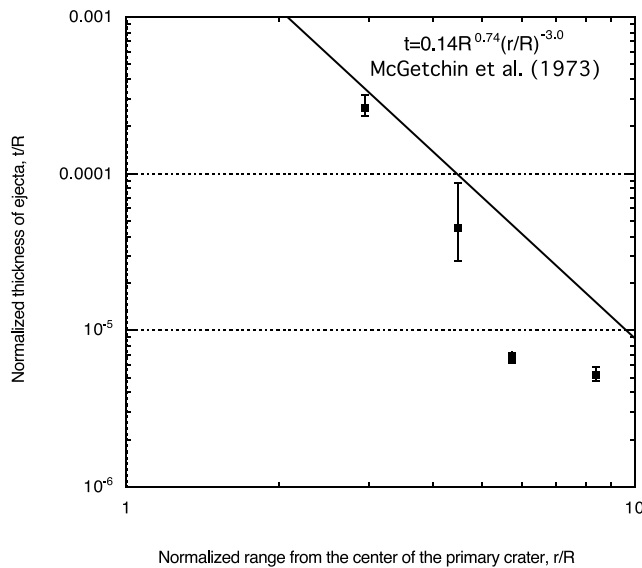
Figure 7. Estimated thickness of ejecta normalized by the radius of the primary crater and comparison with the model thickness of *McGetchin et al.* [1973].

of *McGetchin et al.* [1973]. The estimated thickness, however, drops extremely in the region E3, with the decay in thickness becoming gentler between regions E3 and E4. *Schultz et al.* [1981] proposed a nonconstant decay model of ejecta thickness with the power index of 4.0 for the near ejecta (r/R < 2.5) and 2.5 for the far ejecta (r/R > 2.5). They also suggested that a low decay index of ejecta thickness is applicable to very large distances (r/R < 30), before a rapid decline. A tendency of the power law index to decrease with range is consistent with the model of *Schultz et al.* [1981], although the apparent decay in power law index for large radial ranges is much smaller than that of the model. If the secondary crater density at distances very far from the primary crater follows the trend presented by *Schultz et al.* [1981], this implies that the secondary crater field of Tycho is more extensive and more dense than is inferred from the constant ejecta decay model. We also estimated the volume of secondary forming fragments to be about 6.7×10^2 km³, 4.7% of the total ejecta volume of the primary crater. This ratio is several times larger than those of other lunar craters estimated by *Melosh* [1989]. Even though it is implied that Tycho was formed by an oblique impact [*Schultz and Anderson*, 1996; *Hirata et al.*, 2004], and an asymmetric concentration of ejecta is observed in the downrange region, the excess of ejecta volume of Tycho in the downrange region cannot completely be explained.

5. Summary

[23] We measured the sizes and ranges of secondary craters around the lunar crater Tycho. The size-frequency distributions of secondaries in regions at different distances from the primary show similar power law distributions with an index ranging from 3.3 to 4.0. The value of the index is in agreement with results from a secondary crater field at a distance of 1000 km from Tycho [*Shoemaker*, 1965] and with those of other primary craters of different diameters [*Wilhelms et al.*, 1978]. This index is also the same as the steepened slope of the typical lunar size–frequency distribution for craters of diameter less than 4 km [*Basaltic Volcanism Study Project*, 1981; *Namiki and Honda*, 2003]. This strongly suggests a large contribution of secondaries to the total size–frequency distribution of small lunar craters. At least, small primaries and secondaries are indistinguishable on the basis of only their size-frequency distribution. The decay index of secondary crater densities with distance from the primary craters is not constant and is small at large distances (less than 2.5 for r > 2.5R). Moreover, the total quantity of secondaries forming ejecta fragments is more than twice large than on other lunar primary craters previously studied. These results imply that there are many small secondary crater fields far from the primary crater. In the farthest region in our investigation (8.4R from the primary crater center), the cumulative density of secondary craters at diameter 1 km is 6.8×10^{-3} km⁻³. Although this density is about one third of that of surrounding pre-Nectarian highland terrain, it is almost 10 times denser than that of a typical Copernican terrain [*Namiki and Honda*, 2003]. These secondaries are apparent and easily excluded from primary crater counting. Since our result shows the minimum density of secondary craters, it is still plausible that there are several hidden secondary craters, which we are not able to recognize as secondaries. A ratio of hidden secondaries to apparent secondaries greater than 0.1 would seriously affect the absolute crater chronology on young terrains. Contributions from secondaries of craters smaller than Tycho are also important. *McEwen et al.* [2005] showed that a 10-km-diameter crater on Mars created $\sim 10^7$ secondary craters 10–200 m in diameter. Recent investigations of the statistics of secondary craters including this paper will provide a fundamental data set for construction of a model to represent a terrain with primary craters with a given size-frequency distribution and secondaries made by their ejecta. The modeled spatial distribution and density of secondary craters will make it possible to evaluate precisely the effect of secondary craters on crater counting and chronology.

[24] The estimated relative fragment size distributions are independent of the ejection velocity. This result is the first observational confirmation of theoretical predictions [*O'Keefe and Ahrens*, 1985], and agrees with a recent result from laboratory experiments [*Michikami et al.*, 2005]. The index range of 2.6 to 3.0 for the fragment size distributions is not only close to other natural and experimental craters, but also to that of blocks on the asteroid Eros. The relationship between the maximum fragment size and the ejection velocity is similar to that of crater Copernicus, whose diameter is close to that of Tycho. However, the mean fragment size and estimated total ejecta thickness show a nonconstant decay of fragment number with ejection velocity that reflects a tendency for an absolute size–frequency distribution of secondary craters.

References

Arvidson, R., R. Drozd, E. Guinness, C. Hohenberg, C. Morgan, R. Morrison, and V. Oberbeck (1976), Cosmic ray exposure ages of Apollo 17 samples and the age of Tycho, *Proc. Lunar Planet. Sci. Conf.*, *7th*, 2817–2832.

Basaltic Volcanism Study Project (1981), *Basaltic Volcanism on the Terrestrial Planets*, 1286 pp., Elsevier, New York.

Cheng, A. F. (2004), Collisional evolution of the asteroid belt, *Icarus*, *169*, 357–372.

Cintala, M. J., and R. A. F. Grieve (1998), Scaling impact-melt and crater dimensions: Implications for the lunar cratering record, *Meteorit. Planet. Sci.*, *33*, 889–912.

Fujiwara, A., G. Kamimoto, and A. Tsukamoto (1977), Destruction of basaltic bodies by high-velocity impact, *Icarus*, *31*, 277–288.

Gault, D. E., E. M. Shoemaker, and H. J. Moore (1963), Spray ejected from the lunar surface by meteoroid impact, *NASA TR-D-1767*, Natl. Aeronaut. and Space Admin., Washington, D. C.

Grier, J. A., A. S. McEwen, P. G. Lucey, M. Milazzo, and R. G. Strom (2001), Optical maturity of ejecta from large rayed lunar craters, *J. Geophys. Res.*, *106*, 32,847–32,862.

Hartmann, W. K. (2005), Martian cratering 8: Isochron refinement and the chronology of Mars, *Icarus*, *174*, 294–320.

Haskin, L. A., B. E. Moss, and W. B. McKinnon (2003), On estimating contributions of basin ejecta to regolith deposits at lunar sites, *Meteorit. Planet. Sci.*, *38*, 13–33.

Hirase, Y., A. M. Nakamura, and T. Michikami (2004), Ejecta size-velocity relation derived from the distribution of the secondary craters of kilometer-sized craters on Mars, *Planet. Space Sci.*, *52*, 1103–1108.

Hirata, N., A. M. Nakamura, and K. Saiki (2004), Ejecta and secondary crater distributions of Tycho Crater: Effects of an oblique impact, *Lunar Planet. Sci.* [CD-ROM], XXXV, abstract 1587.

Holsapple, K. A., and R. M. Schmidt (1982), On the scaling of crater dimensions: II. Impact processes, *J. Geophys. Res.*, *87*, 1849–1870.

Hörz, F., R. Ostertag, and D. A. Rainey (1983), Bunte Breccia of the Ries: Continuous deposits of large impact craters, *Rev. Geophys.*, *21*, 1667–1725.

Isbell, C. E., E. M. Eliason, K. C. Adams, T. L. Becker, A. L. Bennett, E. M. Lee, A. S. McEwen, M. S. Robinson, J. R. Shinaman, and L. A. Weller (1999), Clementine: A multi-spectral digital image model archive of the Moon, *Lunar Planet. Sci.*, [CD-ROM], XXX, abstract 1812.

McEwen, A. S. (2003), Secondary cratering on Mars: Implications for age dating and surface properties, paper presented at Sixth International Conference on Mars, Calif. Inst. of Technol., Pasadena.

McEwen, A. S., B. S. Preblich, E. P. Turtle, N. A. Artemieva, M. P. Golombek, M. Hurst, R. L. Kirk, D. M. Burr, and P. R. Christensen (2005), The rayed crater Zunil and interpretations of small impact craters on Mars, *Icarus*, *176*, 351–381.

McGetchin, T. R., M. Settle, and W. Head (1973), Radial thickness variation in impact crater ejecta: Implication for lunar basin deposits, *Earth Planet. Sci. Lett.*, *20*, 226–236.

Melosh, H. J. (1984), Impact ejection, spallation, and the origin of meteorites, *Icarus*, *59*, 234–260.

Melosh, H. J. (1989), *Impact Cratering: A Geologic Process*, Oxford Univ. Press, New York.

Michikami, T., K. Moriguchi, and R. Nakamura (2005), Application to large blocks on asteroid 25143 Itokawa: Ejecta mass distribution with low velocity for impact cratering experiment on porous target, *Lunar Planet. Sci.* [CD-ROM], XXXVI, abstract 1729.

Namiki, N., and C. Honda (2003), Testing hypotheses for the origin of steep slope of lunar size–frequency distribution for small craters, *Earth Planets Space*, *55*, 39–51.

Neukum, G. (1977), Different ages of lunar light plains, *Moon*, *17*, 383–393.

Neukum, G., and B. A. Ivanov (1994), Crater size distributions and impact probabilities on Earth from lunar, terrestrial-planet, and asteroid cratering data, in *Hazards Due to Comets and Asteroids*, edited by T. Gehrels, pp. 359–416, Univ. of Ariz. Press, Tucson.

Oberbeck, V. R. (1975), The role of ballistic erosion and sedimentation in lunar stratigraphy, *Rev. Geophys.*, *13*, 337–362.

Oberbeck, V. R., and R. H. Morrison (1973), On the formation of the lunar herringbone pattern, *Proc. Lunar Planet. Sci. Conf.*, *4th*, 107–123.

O'Keefe, J. D., and T. J. Ahrens (1985), Impact and explosion crater ejecta, fragment size, and velocity, *Icarus*, *62*, 328–338.

Schultz, P. H., and R. R. Anderson (1996), Asymmetry of the Manson impact structure: Evidence for impact angle and direction, in *The Manson Impact Structure, Iowa: Anatomy of an Impact Crater*, *GSA Spec. Pap. 302*, edited by C. Koeberl, pp. 397–417, Geol. Soc. of Am., Boulder, Colo.

Schultz, P. H., and J. Singer (1980), A comparison of secondary craters on the Moon, Mercury and Mars, *Proc. Lunar Planet. Sci. Conf.*, *11th*, 2243–2259.

Schultz, P. H., D. Orphal, B. Miller, W. F. Borden, and S. A. Larson (1981), Multi-ring basin formation: Possible clues from impact cratering calculations, *Proc. Lunar Planet. Sci. Conf.*, *12th, Part A*, 181–195.

Shoemaker, E. M. (1965), Preliminary analysis of the fine structure of the lunar surface in Mare Cognitum, in *Ranger VII Part II: Experimenters' Analyses and Interpretations*, *NASA TR 32-700*, pp. 75–132, Natl. Aeronaut. and Space Admin., Washington, D. C.

Thomas, P. C., J. Veverka, M. S. Robinson, and S. Murchie (2001), Shoemaker Crater as the source of most ejecta blocks on the asteroid 433 Eros, *Nature*, *413*, 394–396.

Vickery, A. M. (1986), Size-velocity distribution of large ejecta fragments, *Icarus*, *67*, 224–236.

Vickery, A. M. (1987), Variation in ejecta size with ejection velocity, *Geophys. Res. Lett.*, *14*, 726–729.

Wilhelms, D. E. (1987), Geologic history of the Moon, *U.S. Geol. Surv. Prof. Pap.*, *1348*, 302 pp.

Wilhelms, D. E., V. R. Oberbeck, and H. R. Aggarwal (1978), Size-frequency distributions of primary and secondary lunar impact craters, *Proc. Lunar Planet. Sci. Conf.*, *9th*, 3735–3762.

———————————

N. Hirata and A. M. Nakamura, Graduate School of Science and Technology, Kobe University, Nada, Kobe 657-8501, Japan. (narunaru@kobe-u.ac.jp)